Frequency Regulation Model of Bulk Power Systems with Energy Storage

N. Sofia Guzman E., *Member, IEEE*, Claudio A. Caizares, *Fellow, IEEE*, Kankar Bhattacharya, *Fellow, IEEE*, and Daniel Sohm, *Member, IEEE*

Abstract—This paper presents a dynamic Frequency Regulation (FR) model of a large interconnected power system including Energy Storage Systems (ESSs) such as Battery Energy Storage Systems (BESSs) and Flywheel Energy Storage Systems (FESSs), considering all relevant stages in the frequency control process. Communication delays are considered in the transmission of the signals in the FR control loop and ESSs, and their State of Charge (SoC) management model is considered. The system, ESSs and SoC components are modelled in detail from a FR perspective. The model is validated using real system and ESSs data, based on a practical transient stability model of the North American Eastern Interconnection (NAEI), and the results show that the proposed model accurately represents the FR process of a large interconnected power network including ESS, and can be used for long-term FR studies. The impact of communication delays and SoC management of ESS facilities in the Area Control Error (ACE) is also studied and discussed.

Index Terms—Area Control Error, batteries, communication delays, energy storage, flywheels, frequency regulation, frequency response.

I. INTRODUCTION

IGH levels of penetration of Renewable Energy Sources (RESs) are increasing the operational challenges in power grids. Most of the challenges are linked to the uncertainty associated with RES, which leads to increased generation/load mismatches that particularly impact Frequency Regulation (FR) and stability. Energy Storage Systems (ESSs) can help to maintain grid stability and reliability [1], [2], providing energy arbitrage, and ancillary services such as FR, among others, while being competitive and economically viable [3], [4].

In recent years, there has been a significant interest in ESSs because of their decreasing costs [5]. Policies around the world are being modified, and new services are being created to facilitate participation of ESSs in the electricity markets [1], [6], [7]. In some instances, Independent System Operators (ISOs) are implementing grid-scale ESS projects to gain experience and evaluate the benefits and performance of different ESS technologies. For instance, the Alternate Technologies for Regulation (ATR) program by the Independent

This work has been submitted to the IEEE for possible publication. Copyright may be transferred without notice, after which this version may no longer be accessible. This work was supported by the NSERC Energy Storage Technology (NEST) Network. The energy storage data was kindly provided by NRStor Inc.

N. S. Guzman, C. A. Cañizares, and K. Bhattacharya are with the Electrical & Computer Engineering Dept., University of Waterloo, Waterloo, ON, N2L 3G1, Canada (e-mail: nguzman@uwaterloo.ca; ccanizares@uwaterloo.ca; kankar.bhattacharya@uwaterloo.ca). D. Sohm is with the IESO of Ontario, Toronto, ON, M5H 1T1, Canada (e-mail: Daniel.Sohm@ieso.ca).

Electricity System Operator (IESO) of Ontario, which includes a Battery Energy Storage System (BESS) and a Flywheel Energy Storage System (FESS) for FR, was implemented to provide learning opportunities for all stakeholders [7].

The fast power response characteristic of ESSs, such as FESS and BESS, make them particularly suitable to provide fast FR services [4]. Studies focusing on ESSs for the provision of FR examine their contribution in helping conventional generators [8] and RES [9] to meet FR requirements, or provide FR themselves (e.g. [10]). However, appropriate ESS models for frequency stability studies are lacking, which hampers the impact analysis studies of ESSs for FR from the ISO perspective.

The model of a two-area system with ESSs used for FR is presented in [11] from the system viewpoint; however, communication delays and State of Charge (SoC) models of the ESS facilities are not considered, which may lead to unrealistic effects in the Area Control Error (ACE). The study in [12] includes communication delays in the FR process, but ESSs are not included, and while [13] considers the SoC model of ESS, the work does not consider communication delays.

Determining the actual and potential benefits of ESSs for FR in an interconnected power system requires a model that represents the overall frequency dynamics of the system and its limitations. The current paper contributes to the on-going efforts of modelling a bulk power system including ESS technologies for FR, as follows:

- Develop the FR model of a large interconnected power grid, estimating the system model parameters, and validating it with real system information.
- Develop empirically-based SoC models for FESS and BESS considering the charging and discharging process characteristics, validating them using data from actual facilities.
- Analyze the impact of communication delays on the ACE and the provision of FR services by ESS facilities.

The rest of the paper is organized as follows: Section II provides a practical overview of frequency control and regulation in power systems, and reviews the ESS technologies used for such services. Section III presents the proposed system and ESS FR models, and Section IV validates the models using real data from the Ontario Power System (OPS), two ESS facilities, and a model of the North American Eastern Interconnection (NAEI). Studies of the impact of communication delays, and the SoC management model of ESS facilities are also presented in Section IV. Finally, Section V highlights the main conclusions and contributions of this paper.

II. BACKGROUND REVIEW

A. Overview of Frequency Control in Power Systems

Frequency is a system-wide characteristic of power grids and should be maintained within specified limits to ensure the stable and reliable operation of the system. Therefore, appropriate frequency control is essential to maintain the normal operation of the grid. FR services are required in order to compensate for forecast errors, non-linear behaviour of demand between dispatches, and generation/load resources that do not follow dispatch instructions. These uncertainties may exceed the contracted capacity of FR resources, which is automatically compensated by the grid inter-ties, thereby deviating the interchanges from their scheduled values [14].

Primary frequency control is critical for maintaining the reliability of the interconnection after a disturbance, by restoring the generation-load balance, and it is implemented through governor control and automatically assisted by the response of frequency dependent loads [14]. Primary control stabilizes the system frequency at a different value from the scheduled one, with the turbine-governor closed loop control being the main component [15]. Thus, there is a need to correct the generation-demand mismatch created by steadystate frequency deviations, which is provided by the dispatched generators in the control area and units that could be started up in short time periods. This action, known as secondary control, has the objective to bring the frequency error back to zero to restore the primary control capability of the system, modifying the power reference of the generators that participate in this control, which is referred as Automatic Generation Control (AGC), and maintaining the ACE within an acceptable range by controlling multiple generators. The ACE extracts contributions of a control area to the interconnection frequency deviation, monitoring and keeping it within limits [14], [15].

B. Overview of Frequency Control in Ontario

In order to maintain the reliability of the power system, the IESO procures ancillary services, FR being one of them. This service seeks to match the generation and load, including losses, to reduce the deviations in the system frequency. Seven generation facilities (hydro and gas) plus two ATR units are contracted by the IESO to provide FR. A minimum requirement of ± 100 MW of AGC with a ramp rate of 50 MW/min must be scheduled every hour [16].

Historically, FR service has been provided by traditional facilities with AGC, which change their output in response to the regulation signals. In 2012, the IESO included the participation of alternative technologies, such as aggregate loads, FESS, and BESS to evaluate their ability to provide FR as compared to the existing facilities [17]. The IESO procured 6 MW for FR from two ESS facilities in 2012, which provide FR services exclusively, thus receiving a regulation signal to reduce the system generation-load mismatch in seconds. The reason for including these ATR units was the need for increasing the FR capacity [17], which are being complemented by another 50 MW ESS capacity under the 2014 Grid Energy Storage Procurement plan [7].

In 2015, the IESO scheduled a minimum of ± 100 MW every hour for FR services, a need which was anticipated to increase due to the increasing penetration of intermittent generation, and only compensated for 53% of the forecast errors; this is expected to further decrease to 40% by 2020, resulting in increased dependency on the power from tie-lines [18]. In 2016, the IESO determined a need for additional FR capacity and one of the ways to reach this target is through the 2017 Request for Proposals (RFP) for incremental regulation capacity, which seeked to increase the FR capacity while being open to different technologies. However, the IESO no longer has contracts with the two facilities. A procurement to acquire FR capacity is being considered by the IESO [19].

2

C. Overview of Energy Storage Systems

ESSs draw energy from the power system, convert it to another form of energy, and release it back to the system when needed. ESSs suitable for FR are those with fast response characteristic, since they can accurately follow the FR signal. Since, BESSs are able to modify their output in less than one second, it makes them a good fit for FR provision, with efficiencies depending on the type (flow or solid state), in the order of 75% to 95%; they also have long lifetimes and low energy density [4]. Another type of ESS apt for FR provision is FESS, which is capable of responding in milliseconds to minutes, have long life cycles, insensitivity to deep discharges, and high round-trip efficiency (90-95%) [4].

III. PROPOSED FR MODEL

To determine a baseline FR model of a real large interconnected power system and estimate the model parameters for a physical system, for which operational information is available, power system analysis tools, such as Dynamic Security Assessment Tools (DSAToolsTM) used by the IESO [20], can be used, as these provide accurate results by properly modelling the system components. Large number of events in one contingency definition (i.e., load changes and FR signal sent to Traditional Generators (TGs) and ESS facilities) with one second between events limits the simulation time; for example, using DSAToolsTM to model and simulate load changes in the entire NAEI and the FR signal sent to a group of generators in one area, limits the maximum simulation time to 102 seconds. However, longer simulation time periods are needed for some frequency studies, such as to calculate the Control Performance Standard 1 (CPS1) or Balancing Authority ACE Limit (BAAL) [21]. Therefore, the model proposed in this paper and depicted in Fig. 1, which includes the main stages in the FR control process, can be used for accurate long-term studies, i.e., hours, days, or even years. The model presented here was developed with the help of the IESO, based on their recommendations and observations of the various signals provided, and through a trial and error approach, using real data. This was implemented in Simulink® [22], with the parameters within each block being determined using the Parameter Estimator application available in this software.

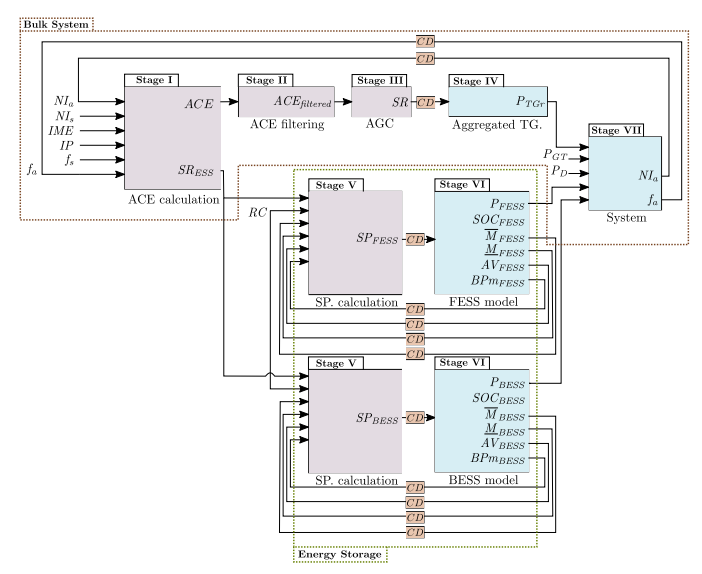


Fig. 1: Frequency response model of a large interconnected power system with FESS and BESS.

A. Bulk Power System

The model in Fig. 1 is based on IESO's approach to FR, with seven stages that capture the most relevant aspects of the frequency control process of a large interconnected power system. It includes communication delays in the signals sent from/to the control center to/from the facilities contracted for regulation, which can significantly impact the FR process depending on the magnitude of the delay; for example, for the IESO, based on the available data, the average value of the one-way communication delay is about 4 s. However, this is not the case for all the facilities; the medium used to transmit the signals and the physical distance from the sending to the receiving point of the signal proportionally affect the delay. Based on the available data, an extra communication delay CD is included in the aggregated model of TG contracted for regulation. The aftereffect of this is an ACE signal that deviates from zero, and in the worst case scenario, the FR signal could worsen the ACE. For example, it could happen that at time t, the system requires a positive regulation action from the FR assets; however, due to CD, the regulation coming from the facilities could be negative, as a result of calculations based on the state of the system at a time t - CD; thus, increasing the ACE. Therefore, delays play an important role in the FR control process and thus should be modeled.

1) ACE Calculation: This is the first stage of the frequency control process. The inputs of this block are the actual power in the interconnection NI_a , and actual frequency f_a , which are the outputs of the system block; the scheduled power in the interconnection NI_s and scheduled frequency f_s change over time and are set by the ISO based on the system's needs; the inadvertent payback IP also changes over time and is set by the ISO; and the interchange metering error IME, which in this case is in manual mode set to -35 MW by the IESO. The block has two outputs: the ACE signal and the SR_{ESS} signal, calculated as follows:

$$ACE = (NI_a - NI_s) - 10B(f_a - f_s) - IME - IP - f(IP)$$
 (1)

$$SR_{ESS} = (NI_a - NI_s) - 10B(f_a - f_s) - IME - f(IP)$$
 (2)



Fig. 2: Stage II ACE filtering block.

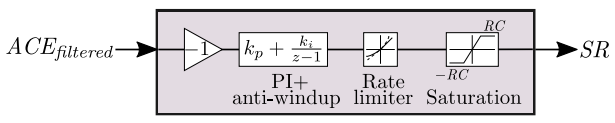


Fig. 3: Stage III AGC.

where the Balancing Authority (BA) bias B is equal to $-248.2~\mathrm{MW}/0.1\mathrm{Hz}$ for the IESO.

The f(IP) function in (1) and (2) is introduced to represent the differences between the measured data and the model results, and is associated with the IP signal. This function is modelled here with a Neural Network (NN), using three signals as inputs: IP_t , IP_{t-10} , and $IP_t - IP_{t-10}$. The NN consists of two layers of 48 neurons and 1 neuron, respectively, with a tangent sigmoid as the activation function. The NN inputs are normalized between -1 and 1 before entering the training process, and the output is converted back to its real scale. One year data was used to obtain the NN model: 80% for training, 10% for testing, and 10% for validation.

- 2) ACE Filtering: This corresponds to Stage II in the FR process and is presented in Fig. 2. The input of this block is the ACE signal from Stage I, and includes a gain c_f and a first order Butterworth filter with a pre-warping frequency ω_0 . The purpose of this filter is to get rid of fast signal changes, since TGs are not able to react to them.
- 3) AGC: It corresponds to Stage III in the FR control process, and is depicted on Fig. 3. The input of this block is the filtered ACE signal from Stage II, and includes an initial negative gain, because the compensation provided by FR should be in the opposite direction to reduce the error. This signal goes into a discrete PI controller with parameters k_p and k_i , and clamping as anti-windup method. The output of the PI block goes through a rate limiter to ensure the generation changes are within limits defined by the ISO $(\pm 50 \text{ MW/min})$ for the IESO), and feeds a saturation block to avoid exceeding the contracted regulation capacity $\pm RC$. The output of this block is the scheduled FR signal SR, sent to the TGs contracted for regulation.
- 4) Aggregated TG: It corresponds to Stage IV in the frequency control process, and is illustrated in Fig. 4. Since the real signal available is the aggregated response of all the TGs to the SR signal, an aggregated model of these TGs is needed; the input of this block is the SR signal from Stage III plus the communication delay CD associated with the FR signal, as previously discussed. The delay in the signals in proportional to the physical distance from the control center to the facilities; after analyzing the data available, an extra communication delay CD_{TG} is included in this model (30 s for the IESO). The third order transfer function TG(z)represents the action of the TGs contracted for regulation, and can be readily estimated from actual measurements. The rate limiter, similar to that in Stage III, ensures the output of this model matches the real data by avoiding unrealistic power changes in the output of the TG group.

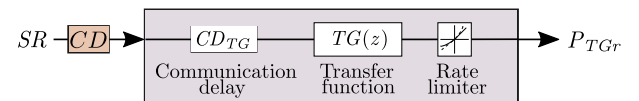


Fig. 4: Stage IV Aggregated model of TG contracted for FR.

5) System Model: It represents the primary frequency response of the elements in the system and the power in the tie-lines, and corresponds to Stage VII in the FR control process. It has five inputs: the load of the system P_D ; the generation total dispatch P_{GT} ; and the outputs of the facilities contracted for regulation P_{TGr} , P_{FESS} , and P_{BESS} . This block calculates the actual frequency f_a and power in the interconnection NI_a at time t, as follows:

$$f_{at} = f_{a0} + \left[-\Delta P_{Dt} + \Delta P_{GTt} + \Delta P_{TGrt} + \Delta P_{FESSt} + \Delta P_{BESSt} \right] \left[\frac{-1}{B_{EI}} \frac{1}{z - 1} - F(z) \right]$$
(3)

$$NI_{at} = NI_{a0} + \left[-\Delta P_{Dt} + \Delta P_{GTt} + \Delta P_{TGrt} + \Delta P_{FESSt} + \Delta P_{BESSt} \right] \left[\frac{B_{EI} - B}{B_{EI}} \frac{1}{z - 1} \right]$$
(4)

which include the same BA bias of (1) and (2), and an NAEI bias B_{EI} calculated from [23], using available data and a detailed transient stability model. In (3), the function F(z) allows obtaining a closer fit between the model results and the measured data.

B. Energy Storage

1) Set-point Calculation: This is Stage V in the FR control process, and includes the calculation of the Set-Point (SP) signals SP_{FESS} and SP_{BESS} sent from the control center to the FESS and BESS facilities, respectively. The calculation of both SP signals is as follows, with the inputs changing for each facility:

$$SP_{ESS} = \begin{cases} \frac{1}{2} (\overline{M}_{ESS} - \underline{M}_{ESS}) \frac{min(SR_{ESS}, RC)}{RC} + BPm_{ESS} \\ \forall AV_{ESS} = 1, RC \neq 0 , SR_{ESS} \geq = 0 \\ \frac{1}{2} (\overline{M}_{ESS} - \underline{M}_{ESS}) \frac{max(SR_{ESS}, -RC)}{RC} + BPm_{ESS} \\ \forall AV_{ESS} = 1, RC \neq 0 , SR_{ESS} < 0 \end{cases}$$
(5)

where AV_{ESS} is the status availability of the facility, \underline{M}_{ESS} and \overline{M}_{ESS} are the minimum and maximum available capacity of the facility, respectively, and BPm_{ESS} is the moving basepoint, which is modelled as the fixed base point of the facility BP_{ESS} moving between \underline{M}_{ESS} and \overline{M}_{ESS} , as illustrated in Fig. 6b, and containing SoC information. Since these signals come from the ESS facilities, communication delays are considered before they arrive at the control center, as shown in Fig. 1. In addition, the FR capacity limit RC, and the SR_{ESS} signal are required in this calculation. The SP_{ESS} signal is in essence a scaled version of the SR_{ESS} signal that takes into account the SoC of the ESS facility reflected through the \overline{M}_{ESS} , M_{ESS} , and BPm_{ESS} signals.

2) ESS Model: This is Stage VI in the frequency control process and includes the ESS models of the BESS and FESS facilities, as well as their SoC management model. Considering that similar operational data was available for the BESS and FESS facilities, similar ESS models were developed

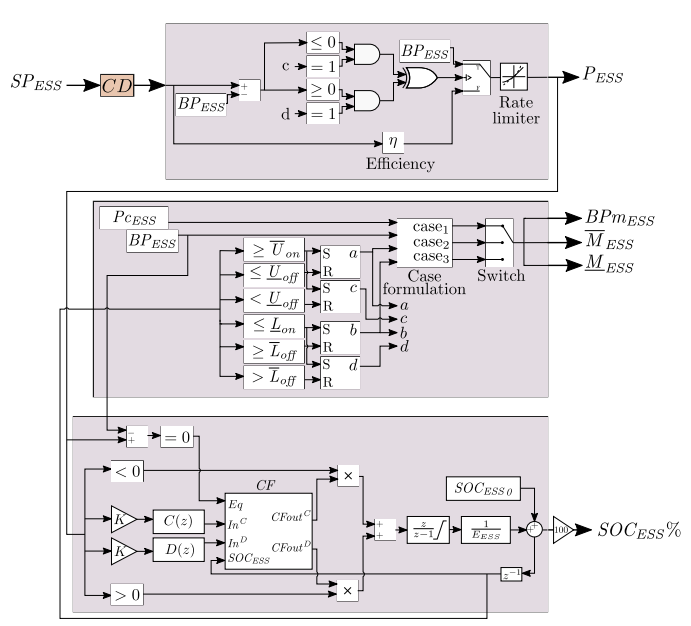


Fig. 5: Stage VI base ESS model including SoC management.

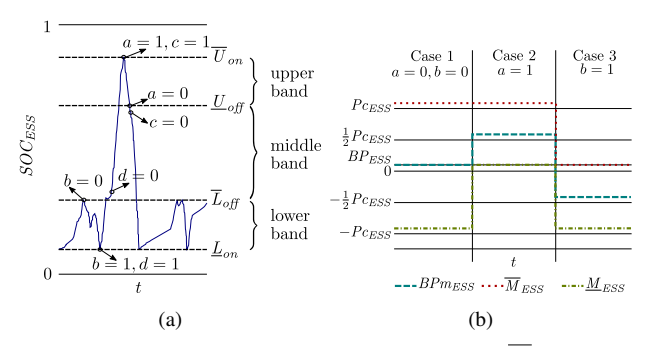


Fig. 6: Relation of (a) parameters a, b, c, and d, and (b) \overline{M}_{ESS} , \underline{M}_{ESS} , and BP_{ESS} to the SoC management of the ESS model.

for both facilities, with different parameters and some specific features for each facility.

Fig. 5 illustrates the base ESS model, which has two main parts: The first part, which is the output of the ESS facility in megawatts, depends on the sign of the regulation required from the facility $(SP_{ESS} - BP_{ESS})$, and the SoC parameters c and d. As shown in Fig. 5, the output signal could be equal to BP_{ESS} or to the delayed SP signal coming from Stage V, and primarily considers the efficiency of the ESS. The output signal goes through a ramp rate block with rising slew rate Rsr, and falling slew rate Fsr. A 100% charging and discharging efficiency η is considered because the actual facility internally compensates the set-point signal taking into account its real efficiency; hence, from the system's perspective, the ESS acts at full efficiency.

The second part of the model is the SoC management of the facility, and it is divided in two sections. In the first section, BPm_{ESS} , \overline{M}_{ESS} , and \underline{M}_{ESS} , and the four SoC parameters a, b, c, and d are calculated. Furthermore, three sections of the SoC are considered: a lower band from \underline{L}_{on} to \overline{L}_{off} , a middle band from \overline{L}_{off} to \underline{U}_{off} , and an upper band from \underline{U}_{off} to \overline{U}_{on} . The parameters a, b, c, and d are directly related to these SoC bands, as illustrated in Fig. 6a and in the second block of Fig. 5. If the output of the ESS causes the SoC to

parameters, which multiply In^D , according to the conditions in (10). The variables k_{up} and k_{dw} are the outputs of set-reset

 $k_{dwt} = S_{dwt} + k_{dwt-1}(R_{dwt} \times -1)$

 $S_{un_{+}} = 1 \ \forall \ SOC_{ESS} \ge ks_{un}$

flip-flops defined as follows:

where

reach \underline{L}_{on} (b=1) or \overline{U}_{on} (a=1), the ESS starts charging or discharging, respectively, despite the regulation signal. This behaviour continues until the SoC reaches \overline{L}_{off} (b=0) or \underline{U}_{off} (a = 0), during the charging/discharging operations, correspondingly.

$$k_{up_t} = S_{up_t} + k_{up_{t-1}}(R_{up_t} \times -1)$$
 (11)

5

(12)

(13)

After the SoC parameters are calculated, and considering the power capacity and base-point of the facility designated for regulation, i.e., Pc_{ESS} , and BP_{ESS} signals, respectively, middle band of Fig. 6a, where a = 0 and b = 0; the second

three cases are formulated. Case 1 considers the SoC in the case considers a = 1, and the third case considers b = 1. The signals BPm_{ESS} , \overline{M}_{ESS} , and \underline{M}_{ESS} , illustrated in Fig. 6b, are calculated as follows:

$$P = 1 \ \forall \ SOC \qquad \langle \ lm \qquad (14)$$

$$BPm_{ESS} = \begin{cases} BP_{ESS} & \forall \quad a = 0, b = 0 \\ BP_{ESS} + Pc_{ESS} & \forall \quad a = 1 \\ BP_{ESS} - Pc_{ESS} & \forall \quad b = 1 \end{cases}$$
 (6)

$$R_{up_t} = 1 \ \forall \ SOC_{ESS} \le kr_{up} \tag{14}$$

$$\overline{M}_{ESS} - Pc_{ESS} \quad \forall \quad b = 1$$

$$\overline{M}_{ESS} = \begin{cases} BP_{ESS} + \frac{1}{2}Pc_{ESS} & \forall \quad a = 0, b = 0 \\ BP_{ESS} + Pc_{ESS} & \forall \quad a = 1 \\ BP_{ESS} & \forall \quad b = 1 \end{cases}$$

$$\underline{M}_{ESS} = \begin{cases} BP_{ESS} - \frac{1}{2}Pc_{ESS} & \forall \quad a = 0, b = 0 \\ BP_{ESS} & \forall \quad a = 1 \\ BP_{ESS} - Pc_{ESS} & \forall \quad b = 1 \end{cases}$$

$$(8)$$

$$S_{dwt} = 1 \ \forall \ SOC_{ESS} \le ks_{dw} \tag{15}$$

$$\underline{M}_{ESS} = \begin{cases}
BP_{ESS} - \frac{1}{2}Pc_{ESS} & \forall \quad a = 0, b = 0 \\
BP_{ESS} & \forall \quad a = 1 \\
BP_{ESS} - Pc_{ESS} & \forall \quad b = 1
\end{cases}$$
(8)

 $R_{dwt} = 1 \ \forall \ SOC_{ESS} > kr_{dw}$ (16)

The second section of the SoC management model is the SoC calculation itself, with the ESS output power P_{ESS} , and the base-point signal BP_{ESS} as inputs, as illustrated in the last block of Fig. 5. The constant K is the power-to-energy value subject to the sampling-time resolution, which in this case is K = -1/3600 hr/s. Thus, $P_{ESS}K$ is the preliminary charge/discharge energy per sampling-time, which is equivalent to a simplified Coulomb counting SoC method [24]. Additionally, the model assumes two second order transfer functions to account for the different charging/discharging characteristics C(z) and D(z), respectively, of the ESS facilities. The outputs of these blocks In^{C} and In^{D} , correspondingly, are inputs of the correction factor CF block in Fig. 5, which compensates for different charge/discharge energy rates observed in the data provided after \overline{U}_{on} and \underline{L}_{on} are reached, as the charging/discharging slows or speeds up after reaching these limits. The CF block has a charging ($CFout^C$) and discharging ($CFout^D$) output, which for the FESS can be defined as follows:

and ks_{up} and kr_{up} are estimated parameters that represent the values of the SoC that cause the set S_{up_t} and reset R_{up_t} signals of the flip-flop $k_{up_{+}}$ to become 1. Likewise, ks_{dw} and kr_{dw} are estimated parameters associated with the SoC values that activates the set (S_{dwt}) and reset (R_{dwt}) signals of the flip-flop k_{dwt} , correspondingly.

$$CFout^{C} = \begin{cases} In^{C} & \forall \ k_{up} = 0, \ k_{dw} = 0 \\ In^{C}CF_{eq} & \forall \ Eq = 1, \ (k_{up} = 1 \lor k_{dw} = 1) \\ In^{C}CF_{1}^{C} & \forall \ Eq = 0, \ k_{up} = 1 \\ In^{C}CF_{2}^{C} & \forall \ Eq = 0, \ k_{up} = 0, \ k_{dw} = 1 \end{cases}$$

$$(9)$$

For the case of BESS, the CF block can be defined as follows:

$$CFout^{D} = \begin{cases} In^{D} & \forall \ k_{up} = 0, \ k_{dw} = 0\\ In^{D}CF_{1}^{D} & \forall \ k_{dw} = 1\\ In^{D}CF_{2}^{D} & \forall \ k_{up} = 1, \ k_{dw} = 0 \end{cases}$$
(10)

$$CFout^{C} = \begin{cases} In^{C} & \forall k_{up} = 0, \ k_{dw} = 0 \\ In^{C} \left[\frac{1}{1 + SOC_{BESS}} \right] CF_{1}^{C} & \forall k_{up} = 1 \\ In^{C} \left[1 + SOC_{BESS} \right] CF^{C2} & \forall k_{up} = 0, \ k_{dw} = 1 \end{cases}$$
(17)

 $CFout^{C} = \begin{cases} In^{C} & \forall \ k_{up} = 0, \ k_{dw} = 0 \\ In^{C}CF_{eq} & \forall \ Eq = 1, \ (k_{up} = 1 \lor k_{dw} = 1) \\ In^{C}CF_{1}^{C} & \forall \ Eq = 0, \ k_{up} = 1 \\ In^{C}CF_{2}^{C} & \forall \ Eq = 0, \ k_{up} = 0, \ k_{dw} = 1 \end{cases}$

$$CFout^{D} = \begin{cases} In^{D} & \forall k_{up} = 0, \ k_{dw} = 0\\ In^{D} \left[1 + SOC_{BESS} \right] CF^{D1} & \forall k_{dw} = 1\\ In^{D} \left[\frac{1}{1 + SOC_{BESS}} \right] CF^{D2} & \forall k_{up} = 1, \ k_{dw} = 0 \end{cases}$$
(18)

where CF_1^C , CF_2^C , and CF_1^D , CF_2^D are estimated parameters

that multiply a function of the SoC, and the inputs In^{C} and

 In^D , respectively. The variables k_{up} and k_{dw} in (17) and (18)

The transfer functions C(z) and D(z) both have a parallel

are the same as in (11) and (12).

comparison block (binary variables) to operate in either mode, which are related to the value of P_{ESS} ; these binary variables are multiplied by $CFout^C$ and $CFout^D$, as shown in Fig. 5. Finally, the estimated corrected energy for the sampling interval is integrated and divided by the ESS energy capacity E_{ESS} and added to the initial SoC value to obtain the estimated SoC output at time t. This value is later multiplied by 100% to obtain $SOC_{ESS}\%$ at time t. The SoC empirical model proposed in this paper is derived by analyzing operational data for an actual FESS and a BESS used for FR by the IESO. Note that the SoC model does not consider degradation or cell failure which will impact the output; further data would be required to model such effects.

Currently, the base-point signal BP_{ESS} for the IESO is zero or a value close to zero, set in each ESS facility. However, the control center may replace the BP_{ESS} with the dispatch from the energy market for facilities that are able to simultaneously participate in both markets. In such a situation, the regulation required from the ESS facilities would be in addition to the base-point signal $(SP_{ESS} - BP_{ESS})$, as currently is the case for TGs.

where CF_{eq} , CF_1^C , CF_2^C are estimated parameters that multiply In^{C} , according to the conditions shown in (9). The input Eq takes the value of 1 when the P_{FESS} is equal to BPm_{FESS} . Furthermore, CF_1^D and CF_2^D are estimated

TABLE I: Model Parameters.

Stage II: ACE filtering					
Parameter Value Parameter Value					
c_f	0.974	ω_0 [rad/s]	0.097		
Stage III: AGC					
Parameter Value Parameter Value					
k_i	0.022	k_p	0.42		

Parameter	==
TG(z)	

	$3.78z^3 + 1.47z^2$					
Stage VI: ESS models						
FE	ESS Model	BESS Model				
Parameter	Value	Parameter	Value			
Rsr[MW]	0.6	Rsr[MW]	1.28			
Fsr[MW]	-0.6	Fsr[mw]	-1.28			
\overline{U}_{on}	1	\overline{U}_{on}	0.885			
\underline{U}_{off}	0.75	$\underline{\underline{U}}_{off}$	0.885			
$rac{U}{\overline{L}_{off}}$	0.25	\overline{L}_{off}	0.125			
\underline{L}_{on}	0	\underline{L}_{on}	0.125			
K	-1/3600	K	-1/3600			
C(z)	$\frac{4.23z^2 + 1.06z + 2.8}{z^2 + 0.57z + 0.42}$ $\frac{5.57z^2 + 6.72z + 3.02}{z^2 + 0.72z + 0.81}$	C(z)	$\frac{0.16z^2 + 4.11z + 7.52}{z^2 + 0.93z + 0.54}$			
D(z)	$\frac{5.57z^2+6.72z+3.02}{z^2+0.72z+0.81}$	D(z)	$ \frac{z^2 + 0.93z + 0.54}{2.88z^2 + 3.78z + 4.57} $ $ \frac{z^2 + 0.48z + 0.55}{z^2 + 0.48z + 0.55} $			
CF_1^C	1.22	CF_1^C	0.014			
CF_2^C	0.99	CF_2^C	0.50			
CF_1^D	1.19	CF_1^D	0.51			
CF_2^D	1.10	CF_2^D	0.64			
CF_{eq}	0.35	CF_{eq}	_			
ks_{up}	1	ks_{up}	0.885			
kr_{up}	0.55	kr_{up}	0.884			
ks_{dw}	0	ks_{dw}	0.125			
7	0.00	7	0.144			

kr_{dw}	0.60	kr_{dw}	0.144
	Stage VII: S	System mo	del
Parameter		Value	
F(z)	$\frac{0.51z^5 - 1.97z^4 + 2.31z}{z^5 - 0.45z^4 - 0.77z^3}$	$z^3 + 2.93z^2 - 1$ $z^2 - 0.23z^2 + 0.6$	$\frac{.18z - 2.73}{.z - 0.12}e^{-5}$

IV. VALIDATION OF PROPOSED FR MODEL ON OPS

All the stages in the proposed FR model shown in Fig. 1 were validated using information provided by the IESO, which included a DSAToolsTM model of the NAEI, OPS data, and data from a 2 MW/0.5 MWh FESS, and a 4 MW/2.76 MWh BESS used for FR by the IESO. All the parameter values of the proposed model determined for the OPS are presented in Table I.

A. Test System Validation

The first step in the validation process of the proposed FR model is the validation of frequency response of the DSAToolsTM model, which is referred here as the test system, against real data. This test system is a reduced representation of the NAEI, with a detailed representation of the OPS and a combination of detailed and equivalent aggregated models, depending on their impact and electrical distances, of the external area.

For validation purposes, seven scenarios capturing the frequency response of the OPS were selected based on regulation

TABLE II: Validation of the frequency response of the DSAToolsTM model.

	RMSE [Hz]	MAE [Hz]		RMSE [Hz]	MAE [Hz]
Case 1	0.00101	0.00082	Case 5	0.00279	0.00225
Case 2	0.00103	0.00084	Case 6	0.00183	0.00139
Case 3	0.00186	0.00129	Case 7	0.00470	0.00359
Case 4	0.00592	0.00512			

signal changes. The load changes for the NAEI were determined based on the measured frequency profile and load changes in the OPS; a frequency response value of -2760 MW/0.1 Hz for the NAEI; and the initial powers of the load, generation, and the interconnection for each scenario. The difference between the total expected load change for the NAEI and the total change in the loads in the OPS was proportionally distributed to all the loads in the rest of the interconnection. Furthermore, three hydroelectric generators in the OPS, with enough capacity to follow the regulation signal, were selected for the provision of FR; the regulation signal was equally divided and sent to these generators. Because of the large number of changes per second, the maximum possible simulation time using the DSAToolsTM software is 102 seconds. Since the simulation period is less than two minutes and the dispatch changes every 5 minutes, it was assumed that the generator active powers were fixed for each scenario.

The Root-Mean Squared Error (RMSE) and Mean Absolute Error (MAE) of ACE for the seven cases on March 20, 2018 are presented in Table II, which can be considered acceptable. Thus, this validated OPS test system was used next to validate the system block of the proposed FR model. The difference between the measured data and test system results could be due to the following reasons:

- The value of frequency response used to determine the power changes in the interconnection was assumed to be fixed for all the scenarios. However, with changes in loads, dispatched generators, and connected renewable generators, this value may change depending on the scenario.
- Since the load models are voltage dependent, and their parameters remain fixed during the simulation, while in the actual system these vary, the modelled load powers may not be the same as in the actual system.
- The dynamic file was modified to obtain a more realistic response from the system. However, these modifications may not be an exact representation of the day selected for simulations.

B. FR Model Validation

All the stages in the proposed FR model are validated in this subsection. The data made available by the IESO corresponds to all the signals associated with the proposed FR model (Fig. 1), which has two sections: the bulk system, which includes Stages I to IV, and Stage VII, and the ESS section, which includes Stage V and VI. For the validation of Stage I to Stage IV, one year of data (April-2018 to March-2019) was used. Fig. 7 shows histograms comparing the measured data and the model results for the ACE, SR_{ESS} , SR, and P_{TGr} signals in MW.

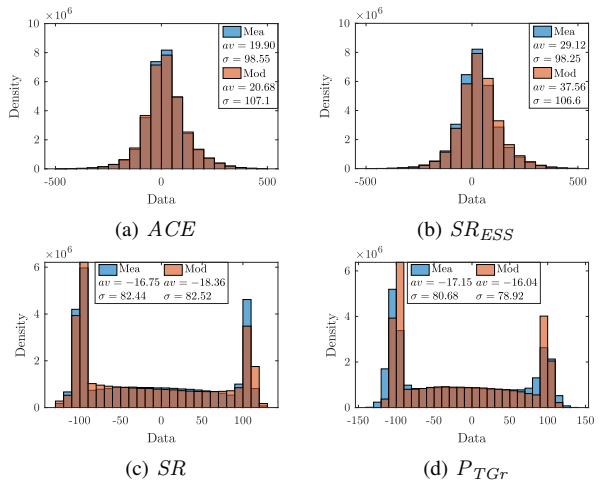


Fig. 7: Histograms of the measured data and model results for Stages I, III and IV.

TABLE III: Estimation errors for f_a and NI_a .

			NI /500	701 34117
	Frequ	iency	$NI_a (523 - 731 \text{ MW})$	
	RMSE [Hz]	MAE [Hz]	RMSE [MW]	MAE [MW]
Case 1	$2.7329e^{-04}$	$2.4423e^{-04}$	4.4963	4.0506
Case 2	$0.9063e^{-04}$	$0.8111e^{-04}$	5.1326	4.1198
Case 3	$1.8753e^{-04}$	$1.5642e^{-04}$	3.9204	3.2470
Case 4	$3.2162e^{-04}$	$2.5331e^{-04}$	15.953	14.161
Case 5	$1.9111e^{-04}$	$1.4437e^{-04}$	5.1016	3.8430
Case 6	$1.0038e^{-04}$	$0.7776e^{-04}$	4.0183	3.3039
Case 7	$0.3653e^{-04}$	$3.0986e^{-04}$	5.3813	4.1019

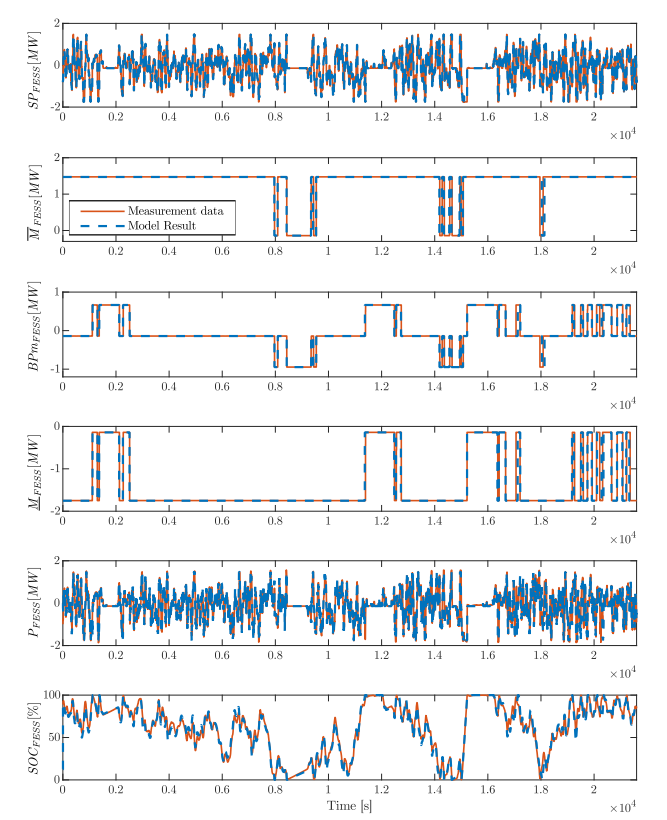


Fig. 8: FESS validation results for February 26, 2020.

After the validation of the frequency response of the test system in the previous subsection, the Stage VII Simulink

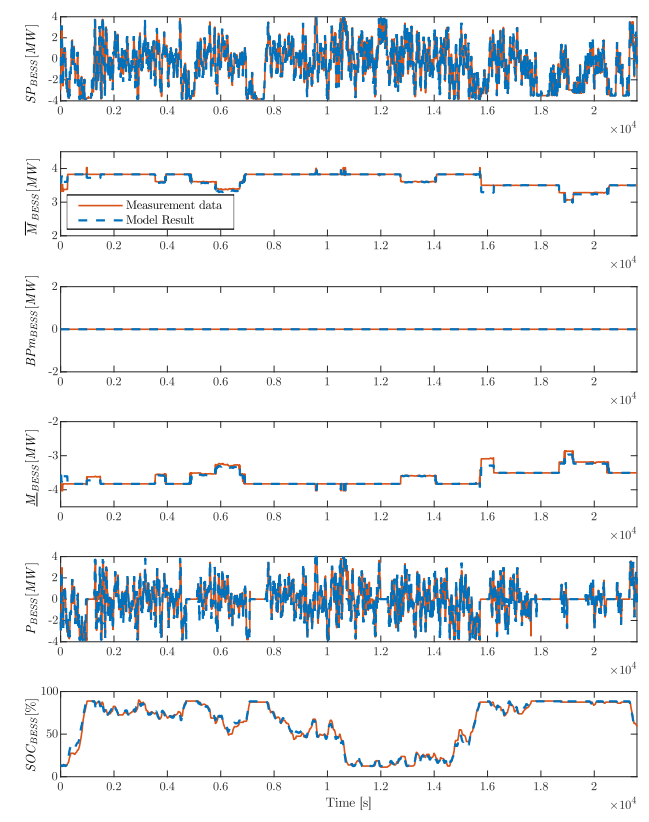


Fig. 9: BESS validation results for January 7, 2020.

model is validated against the test system. Since the measured data of load changes in the neighboring interconnected areas is not available with the same resolution, and considering each BA is mainly responsible for compensating the load changes within its own area, load variations occurring only in the BA of interest are considered here. The same cases used for the validation of the test system were used here, with the difference of no load changes considered in the other BAs within the NAEI. The RMSE and MAE of ACE for the seven cases are presented in Table III. The minimum and maximum NI_s values among the seven cases are 523 and 731 MW, respectively, presented for comparison purposes.

The ESS section of the proposed FR model is validated next. Thus, both Stage V and Stage VI of the FR control process are validated for the FESS and BESS using one day of data for each facility. The target signals are SP_{ESS} from Stage V, and BPm_{ESS} , \overline{M}_{ESS} , \underline{M}_{ESS} , \underline{M}_{ESS} , P_{ESS} and SOC_{ESS} from Stage VI. Simulation results comparing the measured data and the model results for the signals in these two stages are presented in Fig. 8 and Fig. 9 for FESS and BESS, respectively. In these figures, it can be observed that the signals from the proposed FR model closely follow the measurement data from the ESS facilities. For visualization purposes, only a time span of six hours is presented in these figures, while Table IV presents the MAE and RMSE of the FESS and BESS models for a period of one day, for all the signals in the SP calculation and ESS model blocks.

C. Communication Delays

In order to determine the impact of communication delays in the FR process, simulations with existing multiple delays, half

TABLE IV: Estimation errors for FESS and BESS models for a day.

				$\begin{array}{c} BPm_{ESS} \\ [\text{MW}] \end{array}$			
FESS	MAE	0.252	0.041	0.064	0.098	0.204	5.072
(± 2MW)	RMSE	0.425	0.248	0.226	0.390	0.372	7.450
BESS	MAE	0.479	0.045	0.000	0.045	0.330	1.721
(±4MW)	RMSE	0.711	0.102	0.000	0.102	0.609	2.523

TABLE V: Impact of communication delays for 100-day period.

Cases	RMSE [MW]	MAE [MW]
Current delay	87.55	56.91
Half of current delay	84.14	52.50
No delay	80.64	47.12

TABLE VI: Impact of SoC model for 100-day period.

Cases	RMSE [MW]	MAE [MW]
Current ESS for FR (SoC model)	87.55	56.91
30 MW ESS for FR (SoC model)	83.89	52.81
30 MW ESS for FR (no SoC model)	76.98	47.41
80 MW ESS for FR (SoC model)	80.37	49.34

of these delays, and no delays were considered. The impact is measured as a reduction in the ACE. Table V presents the RMSE and MAE with respect to the ideal ACE, i.e., 0 MW. As expected, the smaller the delay, the better is the ACE performance. Note that reducing the communication delays to half their current values has approximately the same effect on the ACE as increasing 30 MW of ESS capacity for FR with the current delay.

D. SoC Management

To demonstrate the effect of the SoC model in the FR control process, the ESS capacity used for FR was increased to 30 MW, comprising a ± 15 MW/30 MWh BESS and a ± 15 MW/3.75 MWh FESS. In the results presented in Table V, it can be observed that ignoring the SoC leads to unrealistic ACE reductions. Indeed, for the IESO case, considering ± 30 MW of fast FR without the SoC model yields a better ACE than increasing the ESS FR capacity to ±80 MW (±40 MW/80 MWh BESS, ± 40 MW/10 MWh FESS) with the SoC model, which could lead to under-procuring fast frequency response resources.

The case of half of existing delays and 30 MW of ESS for FR, including the SoC model, was considered to demonstrate how a combination of reduced communication delays and increased fast FR capacity can realistically reduce the ACE. This reduces the RMSE and MAE of ACE to 81.12 MW and 49.09 MW, respectively.

V. CONCLUSIONS

This paper presented a validated dynamic model for longterm FR studies of a real interconnected power system including ESS facilities. The proposed estimated FR model was designed to closely represent the frequency behaviour of a large interconnected system, and the ESS model allowed an accurate representation of the SoC management and charging/discharging characteristics of FESS and BESS. Simulation results showed that reducing the communication delays can

potentially reduce the ACE without requiring any increase in FR capacity, and that neglecting the SoC model of ESSs in the frequency control process yields unrealistic improvements in the ACE.

REFERENCES

- [1] L. Meng, J. Zafar, S. K. Khadem, A. Collinson, K. C. Murchie, F. Coffele, and G. M. Burt, "Fast frequency response from energy storage systems areview of grid standards, projects and technical issues," IEEE Transactions on Smart Grid, vol. 11, no. 2, pp. 1566-1581, 2020.
- [2] J. P. Barton and D. G. Infield, "Energy storage and its use with intermittent renewable energy," IEEE Trans. Energy Convers., vol. 19, no. 2, pp. 441-448, June 2004.
- C. Byers and A. Botterud, "Additional capacity value from synergy of variable renewable energy and energy storage," IEEE Transactions on Sustainable Energy, vol. 11, no. 2, pp. 1106-1109, 2020.
- [4] "DOE/EPRI electricity storage handbook in collaboration with NRECA," Sandia National Laboratories, Tech. Rep., March 2013.
- [5] "E-storage: shifting from cost to value wind and solar applications," World Energy Council, Tech. Rep., 2016.
- "Electric storage participation in markets operated by regional transmission organizations and independent system operators," FERC, Tech. Rep., 2018.
- "Removing obstacles for storage resources in Ontario," IESO, Tech. Rep., 2018.
- [8] X. Xie, Y. Guo, B. Wang, Y. Dong, L. Mou, and F. Xue, "Improving AGC performance of coal-fueled thermal generators using multi-MW scale BESS: a practical application," IEEE Transactions on Smart Grid, vol. 9, no. 3, pp. 1769-1777, 2018.
- [9] G. He, Q. Chen, C. Kang, Q. Xia, and K. Poolla, "Cooperation of wind power and battery storage to provide frequency regulation in power markets," IEEE Transactions on Power Systems, vol. 32, no. 5, pp. 3559– 3568, 2017.
- [10] J. W. Shim, G. Verbi, N. Zhang, and K. Hur, "Harmonious integration of faster-acting energy storage systems into frequency control reserves in power grid with high renewable generation," IEEE Transactions on Power Systems, vol. 33, no. 6, pp. 6193-6205, 2018.
- [11] S. Pulendran and J. E. Tate, "Capacity scheduling of energy storage and conventional generation for frequency regulation based on CPS1," IEEE Transactions on Power Systems, vol. 35, no. 1, pp. 405-414, 2020.
- [12] H. Bevrani and T. Hiyama, "On loadfrequency regulation with time delays: Design and real-time implementation," IEEE Transactions on Energy Conversion, vol. 24, no. 1, pp. 292-300, 2009.
- [13] Y. Cheng, M. Tabrizi, M. Sahni, A. Povedano, and D. Nichols, "Dynamic available AGC based approach for enhancing utility scale energy storage performance," IEEE Transactions on Smart Grid, vol. 5, no. 2, pp. 1070-1078, 2014.
- [14] "Balancing and frequency control," NERC, Tech. Rep., 2011.
- [15] A. Gomez-Exposito, A. Conejo, and C. Canizares, Electric energy systems analysis and operation. CRC Press, 2018.
- "Market rules for the Ontario electricity market," IESO, Tech. Rep., 2020.
- "Ancillary [17] services market," IESO. 2020, [Accessed: 10th 2020]. Available: http://www.ieso.ca/ June [Online]. sector-participants/market-operations/markets-and-related-programs/ ancillary-services-market
- "2016 IESO operability assessment summary," IESO, Tech. Rep., 2016.
- [19] "Active Engagements: Market Development Advisory Group," IESO, 2020, [Accessed: August 21st, 2020]. [Online]. Available: http://www.ieso.ca/Sector-Participants/Engagement-Initiatives/ Engagements/Market-Development-Advisory-Group [20] "DSATools," Powertech, 2020, [Accessed: June 24th, 2020]. [Online].
- Available: https://www.dsatools.com/
- [21] "BAL-001-2 real power balancing control performance standard background document," NERC, Tech. Rep., 2013.
- [22] "Simulink," Mathworks, 2020, [Accessed: June 24th, 2020]. [Online]. Available: https://www.mathworks.com/products/simulink.html
- [23] "Attachment A, BAL-003-1 frequency response and frequency bias setting," NERC, Tech. Rep., 2012.
- M. Hannan, M. Lipu, A. Hussain, and A. Mohamed, "A review of lithium-ion battery state of charge estimation and management system in electric vehicle applications: Challenges and recommendations," Renewable and Sustainable Energy Reviews, vol. 78, pp. 834-854, 2017.